J. Phys. B: At. Mol. Opt. Phys. **33** (2000) 47–54. Printed in the UK PII: S0953-4075(00)09145-8

Coherence properties of an atom laser

Marek Trippenbach†‖, Y B Band†, Mark Edwards‡, Marya Doery§, P S Julienne§, E W Hagley§, L Deng§, M Kozuma§¶, K Helmerson§, S L Rolston§ and W D Phillips§

† Departments of Chemistry and Physics, Ben-Gurion University of the Negev, Beer-Sheva 84105, Israel
‡ Department of Physics, Georgia Southern University, Statesboro, GA 30458-8031, USA
§ National Institute of Standards and Technology, 100 Bureau Drive Stop 8423, Gaithersburg, MD 20899-8423, USA

Received 2 November 1999

Abstract. We study the coherence properties of an atom laser, which operates by extracting atoms from a gaseous Bose–Einstein condensate via a two-photon Raman process, by analysing a recent experiment (Hagley *et al* 1999 *Phys. Rev. Lett.* **83** 3112). We obtain good agreement with the experimental data by solving the time-dependent Gross–Pitaevskii equation in three dimensions both numerically and with a Thomas–Fermi model. The coherence is strongly affected by the space-dependent phase developed by the condensate when the trapping potential is turned off.

1. Introduction

One of the most exciting prospects resulting from the Bose–Einstein condensation of alkali vapours [1–3] is the possibility of producing an intense, coherent, and directed beam of matter waves, i.e., an atom laser. Indeed, prototype atom lasers have already been demonstrated [4, 5]. Potential atom-laser applications include time-and-frequency standards, atom holography, and nanolithography. A critical element in the operation of an atom laser is the 'output coupler' by which atoms are coherently extracted from the condensate [6]. The design of this element is key to controlling the properties of the atom-laser beam [7]. At least two output-coupler mechanisms have been demonstrated. Condensate atoms have been extracted by radio frequency fields [8, 9] and by two-photon Raman transitions [10]. A quasi-continuous atom laser was demonstrated recently [5] by using a rapid-fire sequence of laser pulses each of which caused condensate atoms to undergo a Raman transition that transferred momentum while simultaneously changing their internal state so that they were not trapped by the magnetic potential. Earlier theoretical studies of the properties of atom lasers [7, 11–13] made no comparisons of theory and experiment. This paper examines the coherence properties of atom-laser wavepackets by analysing a recent NIST experiment [14] which probes such properties by measuring the decay of the interference contrast of two overlapping wavepackets outcoupled from a Na atom condensate and separated by a variable delay time Δt.

‖ Present address: Institute of Experimental Physics, Optics Division, Warsaw University, ul.Hoza 69, Warsaw 00-681, Poland.
¶ Present address: Institute of Physics, University of Tokyo, 3-8-1 Komaba, Meguro-ku, Tokyo 153-8902, Japan.

0953-4075/00/010047+08$30.00

2. Description of experiment

A parent condensate with wavefunction $\Psi_0(\boldsymbol{r}, t_1)$ is prepared at time t_1. In one experiment the harmonic trapping potential was left on all the time, and we take $t_1 = 0$. In another experiment, the trapping potential was turned off and the condensate allowed to expand freely for up to $t_1 = 5$ ms. A 100 ns standing-wave laser pulse was applied at time t_1 with a wavelength $\lambda_L = 589$ nm, detuned 600 MHz to the red of atomic resonance. This first laser pulse diffracts the condensate [15] to make two wavepackets $\psi_1^{\pm}$ moving in the z-direction with momenta $\pm 2\boldsymbol{p}$, where $p = \hbar k = h/\lambda_L$. We consider only the wavepacket with wavevector $+2k$, since the problem is symmetric. At time $t_2 = t_1 + \Delta t$, the wavepacket evolves to

$$\psi_1^+(\boldsymbol{r}, t_2) = \phi_1(\boldsymbol{r}, t_2) \mathrm{e}^{\mathrm{i}2kz} \mathrm{e}^{-\mathrm{i}\frac{4E_R}{\hbar}\Delta t}, \tag{1}$$

where $E_R = \frac{\hbar^2 k^2}{2m}$ and m is the atomic mass. The slowly varying envelope function ϕ_1 is initially just a copy of the parent condensate wavefunction with norm $|\alpha|^2 \ll 1$: $\phi_1(\boldsymbol{r}, t_1) = \alpha \Psi_0(\boldsymbol{r}, t_1)$. In the experiment $|\alpha|^2 \approx 0.02$. The momentum spread of Ψ_0 is very small compared with $2\hbar k$. The first wavepacket moves $\Delta \boldsymbol{z} = \boldsymbol{v}\Delta t$ in time $\Delta t = t_2 - t_1$, where $v = 2\hbar k/m$ is the group velocity (60 μm ms^{-1}). Hence, a good approximation to the slowly varying envelope at time t_2 is given by $\phi_1(\boldsymbol{r}, t_2) = \alpha \Psi_0(\boldsymbol{r} - \Delta \boldsymbol{z}, t_1)$. This approximation does not take into account the diffraction of the envelope nor does it take into account the acceleration of the high-momentum component by the zero-momentum component, as discussed in section 4.

A second standing-wave laser pulse at time $t_2 = t_1 + \Delta t$ creates a second set of wavepackets $\psi_2^{\pm}$, where $\psi_2^+(\boldsymbol{r}, t_2) = \phi_2(\boldsymbol{r}, t_2)\mathrm{e}^{\mathrm{i}2kz}$ and $\phi_2(\boldsymbol{r}, t_2) = \alpha \Psi_0(\boldsymbol{r}, t_2)$. The combined number of atoms in the $+2k$ wavepacket is $\langle |\psi_1^+ + \psi_2^+|^2 \rangle_r$, where the brackets imply an integration over spatial coordinates. This fast $+2k$ wavepacket soon clears the slowly expanding parent condensate and later can be imaged experimentally. The number of atoms in the $+2k$ wavepacket is proportional to the following contrast function $C(t_1, \Delta t)$, defined so as to vary between 0 and 1:

$$C(t_1, \Delta t) \equiv \frac{1}{4\alpha^2} \langle |\psi_1^+ + \psi_2^+|^2 \rangle_r \tag{2}$$

$$= \frac{1}{4} \left\langle \left| \frac{\phi_1(\boldsymbol{r} - \Delta \boldsymbol{z}, t_2)}{\alpha} \mathrm{e}^{-\mathrm{i}\frac{4E_R \Delta t}{\hbar}} + \frac{\phi_2(\boldsymbol{r}, t_2)}{\alpha} \right|^2 \right\rangle_r \tag{3}$$

$$= \tfrac{1}{2} + \tfrac{1}{2}\Gamma(t_1, \Delta t). \tag{4}$$

The correlation function

$$\Gamma(t_1, \Delta t) = \frac{1}{2|\alpha|^2} \langle \psi_1^+ \psi_2^{+*} + \psi_1^{+*} \psi_2^+ \rangle_r, \tag{5}$$

is given by

$$\Gamma(t_1, \Delta t) = \mathrm{Re} \left\langle \frac{\mathrm{e}^{\mathrm{i}\frac{4E_R \Delta t}{\hbar}} \phi_1^*(\boldsymbol{r} - \Delta \boldsymbol{z}, t_2) \phi_2(\boldsymbol{r}, t_2)}{|\alpha|^2} \right\rangle_r . \tag{6}$$

The correlation function $\Gamma(t_1, \Delta t)$ in equation (6) provides a measure of the spatial and temporal coherence of the outcoupled wavepackets. In the hypothetical case that the moving packets are plane waves ($\phi_1 = \phi_2 =$ constant), then $\Gamma(t_1, \Delta t) = \cos(4E_R \Delta t/\hbar)$ varies between $+1$ when the wavepackets are in phase ($4E_R \Delta t/\hbar = 2n\pi$ or $\Delta t = n\tau$, where $\tau = \frac{h}{4E_R} = 10$ μs for Na atoms) and -1 when they are out of phase ($\Delta t = (n + \frac{1}{2})\tau$). The two packets constructively and destructively interfere in these two respective cases, giving a contrast function $C(t_1, \Delta t)$ which changes from 1 to 0 in a time $\Delta t = \tau/2$. Actual condensate wavepackets of finite Thomas–Fermi (TF) radius z_{TF} [16] in the z-direction will physically

separate after times of the order of $t_{\rm TF} = 2z_{\rm TF}/v$, after which $\Gamma \to 0$ and $C(t_1, \Delta t) \to \frac{1}{2}$. Thus $C(t_1, \Delta t)$ oscillates rapidly between 1 and 0 when $\Delta t \ll t_{\rm TF}$ and $\Delta z \ll z_{\rm TF}$, and approaches $\frac{1}{2}$ when $\Delta t > t_{\rm TF}$ and $\Delta z > 2z_{\rm TF}$. We will see that when t_1 is long enough for significant phase modulation to have developed across the condensate due to the mean field term in the Gross–Pitaevskii (GP) equation, then $C(t_1, \Delta t)$ drops to $\frac{1}{2}$ in a time short compared with $t_{\rm TF}$.

In the NIST experiment, the harmonic trap holding the initial condensate had frequencies $\frac{\omega}{2\pi}$ of 14 Hz, $28/\sqrt{2}$ Hz, and 28 Hz in the x-, y-, and z-directions, respectively, and a mean frequency of $\frac{\bar{\omega}}{2\pi} = 28/\sqrt{2}$ Hz. If the parent condensate has 1.5×10^6 atoms, $z_{\rm TF}(x) = 22\ \mu$m and $t_{\rm TF} = 740\ \mu$s. The characteristic time for developing phase modulation (i.e. momentum spread) across the condensate is $1/\bar{\omega} = 8$ ms. The experimental t_1 varied from 0 to 5 ms, and Δt from 0 to around 500 μs. Wavepacket images were taken about 6 ms after t_1, long after the fast wavepacket has cleared the stationary, slowly expanding parent condensate. The number of atoms in the $\pm 2k$ wavepackets could be measured using such images.

The experimental on-resonant absorption imaging technique does not allow the determination of the number of atoms, N, in the parent condensate (because the parent image corresponds to complete absorption of the probe light used for imaging). Therefore, in order to obtain a signal that is not sensitive to shot-to-shot fluctuations in N, the NIST experiment actually utilized a second pair of standing-wave pulses to produce a new set of $\pm 2k$ wavepackets. The first pulse of the second pair was applied at time $t_3 = t_1 + 3$ ms, after the fast wavepackets from the pulse pair at (t_1, t_2) have moved away from the parent condensate. The second pulse of the second pair was applied at $t_4 = t_3 + \Delta t + \tau/2$, where $\tau/2 = 5\ \mu$s. Thus, when $\Delta t \ll t_{\rm TF}$, the contrast function $C_2(t_3, \Delta t + \tau/2)$ for the second pulse pair is exactly out of phase with the contrast function $C_1(t_1, \Delta t)$ for the first pulse pair. The experimental images separately determine the number of atoms in the $\pm 2k$ wavepackets from the (t_1, t_2) and the (t_3, t_4) pulse pairs. The normalization to the number of atoms in each condensate, which varies from shot to shot, is accomplished by calculating the following 'signal' function:

$$S(t_1, t_3, \Delta t) = \frac{C(t_1, \Delta t)}{C(t_1, \Delta t) + C(t_3, \Delta t + \tau/2)}. \tag{7}$$

Just like C, the signal S oscillates rapidly between 0 and 1 for $\Delta t \ll t_{\rm TF}$ and approaches $\frac{1}{2}$ when $\Delta t > t_{\rm TF}$.

A 'coherence time', Δt_c, for the output coupled wavepackets can be defined using the correlation function $\Gamma(t_1, \Delta t)$. The definition of a correlation time is not unique. Two commonly used definitions for correlation times in optics are: $\Delta t_c(t_1) = \int_0^\infty {\rm d}(\Delta t)|\Gamma(t_1, \Delta t)|^2$, and $\Delta t_c^2(t_1) = \int_0^\infty {\rm d}(\Delta t)(\Delta t)^2|\Gamma(t_1, \Delta t)|^2 / \int_0^\infty {\rm d}(\Delta t)|\Gamma(t_1, \Delta t)|^2$. Here we define a coherence time $\Delta t_c(t_1, t_3)$ related to the decay of the signal function $S(t_1, t_3, \Delta t)$. $\Delta t_c(t_1, t_3)$ is the time for the envelope S_e of S to decay halfway from its $\Delta t = 0$ value of 1 to its long time limiting value of $\frac{1}{2}$, that is, $S_e(t_1, t_3, \Delta t_c) = 0.75$. A corresponding 'coherence length' is $\Delta z_c(t_1, t_3) = v\Delta t_c(t_1, t_3)$. The coherence time and length defined here measure the decay of the wavepacket interference due to the unitary time evolution of the zero-temperature condensate wavefunction. In this case there is no decoherence due to the interactions with a bath or due to inelastic processes.

3. Theoretical methods

The time-dependent GP (TDGP) equation describes the dynamics of $\Psi(\boldsymbol{r}, t)$, which includes the parent condensate plus the fast $\pm 2k$ wavepackets:

$$\mathrm{i}\hbar\frac{\partial\Psi}{\partial t} = -\frac{\hbar^2}{2m}\nabla^2\Psi(\boldsymbol{r}, t) + (V_{\mathrm{trap}}(\boldsymbol{r}, t) + V_{\mathrm{laser}}(\boldsymbol{r}, t))\Psi(\boldsymbol{r}, t) + U_0 N\,|\Psi(\boldsymbol{r}, t)|^2\,\Psi(\boldsymbol{r}, t), \tag{8}$$

where $U_0 = 4\pi\hbar^2 a/m$, a is the s-wave scattering length, N is the total number of condensate atoms and $V_{\mathrm{trap}}(\boldsymbol{r}, t)$ is the trapping potential. The contrast functions C_1 and C_2 can be calculated from $\Psi(\boldsymbol{r}, t)$. The interaction of condensate atoms with the four standing-wave laser pulses can be written as

$$V_{\mathrm{laser}}(\boldsymbol{r}, t) = V_L \cos(2\boldsymbol{k}\cdot\boldsymbol{r}) \sum_{n=1}^{4} f(t - t_n), \tag{9}$$

where $V_L f(t)$ is the single laser pulse envelope, and f is normalized such that $\int_{-\infty}^{\infty} \mathrm{d}t f(t) = \delta t$, where δt is the effective laser pulse duration. Here $\delta t = 100$ ns is short compared with Δt. The factors t_n are the times at which the four experimental pulses are applied.

The modification to the condensate wavefunction caused by a short-duration, low-intensity, standing-wave laser pulse can be described well by using the Raman–Nath approximation [17]. Thus we assume that during each light pulse, the light-shift potential energy (9) dominates all other terms in equation (8). The time-evolution operator during any pulse n is then approximated to first order as $1 - \mathrm{i}[V_L\delta t/\hbar]\cos(2\boldsymbol{k}\cdot\boldsymbol{r})$, where the phase shift $V_L\delta t/\hbar \ll 1$ in the experiments under consideration. This operator relates the wavefunction after the laser pulse with that before the pulse in a simple way:

$$\Psi(\boldsymbol{r}, t_n + \delta t) \simeq \Psi_0(\boldsymbol{r}, t_n) - \frac{\mathrm{i}}{2\hbar} V_L\delta t \times [\mathrm{e}^{2\mathrm{i}\boldsymbol{k}\cdot\boldsymbol{r}} + \mathrm{e}^{-2\mathrm{i}\boldsymbol{k}\cdot\boldsymbol{r}}]\Psi_0(\boldsymbol{r}, t_n). \tag{10}$$

The effect can be qualitatively understood in momentum space. Before the first pulse, there is only a component centred at momentum = 0. After the pulse, sidebands that are proportional to the initial wavefunction are present at momentum = $\pm 2\hbar\boldsymbol{k}$. Each subsequent pulse is modelled in the same way, since population in higher-order momentum components is negligible. We have tested equation (10) by numerically solving a one-dimensional (1D) form of the GP equation (8) for a single short pulse. The resulting numerical wavefunction differs only slightly from the closed form solution of equation (10). The $\pm 2\hbar\boldsymbol{k}$ components acquire a very small spatially varying phase in the numerical simulations, which is associated with the mean field effects that have been ignored in developing equation (10). Overall, the description of equation (10) is a very good one.

We have used two different methods to evolve $\Psi(\boldsymbol{r}, t)$. The first is an approximate method which we call the time-dependent TF (TDTF) method. Let us first consider the case when the trapping potential is turned off at $t = 0$ prior to the first pulse at t_1. Once V_{trap} is removed, the parent condensate, $\Psi_0(\boldsymbol{r}, t)$, evolves freely, develops spatial phase variation, i.e. phase modulation, and expands somewhat. The 3D form of $\Psi_0(\boldsymbol{r}, t)$ can be easily found since, for expanding condensates where the TF approximation is valid, the solution of the TDGP is self-similar, i.e., it can be transformed to its original shape (before release) by suitable axis scalings. The time dependence of the scale parameters has been shown [18] to obey coupled nonlinear ordinary differential equations. Once the atoms in high-momentum states clear the parent condensate, they evolve as free particles (if $V_L\delta t/\hbar \ll 1$) and move with velocity $\pm 2\hbar\boldsymbol{k}/m$. In our 3D model, the full condensate wavefunction thus evolves after application of the first

pulse as follows:

$$\Psi(\boldsymbol{r},t) \approx \Psi_0(\boldsymbol{r},t) - \frac{\mathrm{i}}{2\overline{h}} V_L \delta t \mathrm{e}^{-\mathrm{i}4E_R(t-t_1)/\overline{h}} [\mathrm{e}^{2\mathrm{i}\boldsymbol{k}\cdot\boldsymbol{r}} \Psi_0(\boldsymbol{r} - \boldsymbol{v}(t-t_1), t_1) + \mathrm{e}^{-2\mathrm{i}\boldsymbol{k}\cdot\boldsymbol{r}} \Psi_0(\boldsymbol{r} + \boldsymbol{v}(t-t_1), t_1)]. \tag{11}$$

Using equations (10) and (11) we can develop the condensate wavefunction for any number of pulses and delays. When the trap is left on, the main modification to the above analysis is that the parent condensate does not develop phase or expand.

The second method is a numerical propagation of the 3D solution to the TDGP equation using the slowly varying envelope approximation (SVEA) to reduce the grid size. The SVEA is excellent here because the momentum spread $\overline{h}\Delta k_0$ of Ψ_0 is very small compared with $2\overline{h}k$. We have verified that this method gives excellent agreement with full numerical solutions of the TDGP equation in one and two dimensions. Consequently with the SVEA we can efficiently calculate accurate contrast functions for a zero-temperature condensate for any time sequence of the trapping potential and laser pulses.

The SVEA to the GP equation is made by writing the wavefunction as

$$\Psi(\boldsymbol{r},t) = \sum_{l=-1}^{1} \varphi_l(\boldsymbol{r},t) \exp(\mathrm{i}\boldsymbol{k}_l\boldsymbol{r} - \mathrm{i}\omega_l t). \tag{12}$$

Here we have explicitly separated out the fast oscillating phase factors representing central momenta $\boldsymbol{k}_{-1} = -2k\hat{\boldsymbol{z}}$, $\boldsymbol{k}_0 = 0$, $\boldsymbol{k}_1 = +2k\hat{\boldsymbol{z}}$ and kinetic energy $E_l = \overline{h}\omega_l = \overline{h}^2 k_l^2/2\ m$. For example, the component labelled by $l = 1$ represents for $t_1 < t < t_2$ the wavepacket that results from applying the laser pulse at $t = t_1$, whereas for $t > t_2$ it represents the net wavepacket that results from the sequence of both pulses. Since the slowly varying envelopes $\varphi_l(\boldsymbol{r},t)$ vary in time and space on much slower scales than the phase factors, the spatial grid used for numerical simulations of the time evolution of the dynamics can have a step size of the order of $(\Delta k_0)^{-1}$, which is much larger than $(2k)^{-1}$. Substituting the SVEA form of equation (12) for the wavefunction into the GP equation, collecting terms multiplying the same phase factors, multiplying by the complex conjugate of the appropriate phase factors, and neglecting all terms that are not phase matched (i.e. those for which momentum and energy are not conserved), we obtain a set of coupled equations for the slowly varying envelopes $\varphi_l(\boldsymbol{r},t)$:

$$\left(\frac{\partial}{\partial t} - (\overline{h}\boldsymbol{k}_l/m)\cdot\boldsymbol{\nabla} + \frac{\mathrm{i}}{\overline{h}}\left(\frac{-\overline{h}^2}{2m}\nabla^2 + V(\boldsymbol{r},t)\right)\right)\varphi_l(\boldsymbol{r},t) = -\frac{\mathrm{i}}{\overline{h}} U_0 N \sum_{jqs} \delta(\boldsymbol{k}_l - \boldsymbol{k}_j + \boldsymbol{k}_q - \boldsymbol{k}_s)\delta(\omega_l - \omega_j + \omega_q - \omega_s) \times \varphi_j(\boldsymbol{r},t)\varphi_q^*(\boldsymbol{r},t)\varphi_s(\boldsymbol{r},t). \tag{13}$$

Only phase-matched terms (terms for which $\boldsymbol{k}_l - \boldsymbol{k}_j + \boldsymbol{k}_q - \boldsymbol{k}_s = 0$ and $\omega_l - \omega_j + \omega_q - \omega_s = 0$) are retained on the right-hand side of equations (13). The SVEA equations for our case are given explicitly by

$$\left(\frac{\partial}{\partial t} + \frac{\mathrm{i}}{\overline{h}}\left(-\frac{\overline{h}^2}{2m}\nabla^2 + V(\boldsymbol{r},t)\right)\right)\varphi_0 = -\frac{\mathrm{i}}{\overline{h}} U_0 N(|\varphi_0|^2 + 2|\varphi_1|^2 + 2|\varphi_{-1}|^2)\varphi_0, \tag{14}$$

$$\left(\frac{\partial}{\partial t} - (2\overline{h}\boldsymbol{k}/m)\cdot\boldsymbol{\nabla} + \frac{\mathrm{i}}{\overline{h}}\left(\frac{-\overline{h}^2}{2m}\nabla^2 + V(\boldsymbol{r},t)\right)\right)\varphi_1 = -\frac{\mathrm{i}}{\overline{h}} U_0 N(|\varphi_1|^2 + 2|\varphi_0|^2 + 2|\varphi_{-1}|^2)\varphi_1, \tag{15}$$

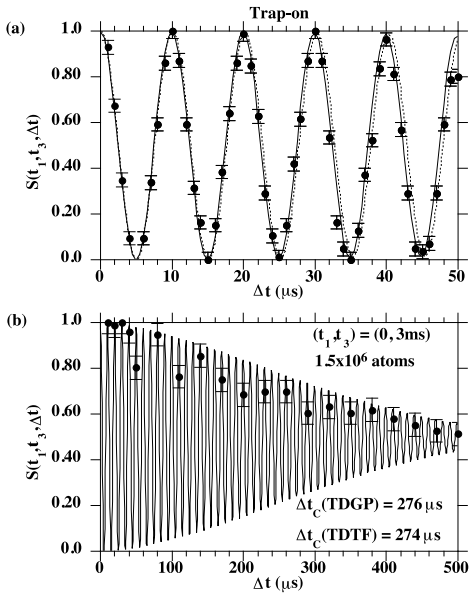

Figure 1. Comparison of calculated TDGP (solid curve) and TDTF (dashed curve) and experimental (points) signal functions $S(t_1 = 0, t_3 = 3\ \text{ms}, \Delta t)$ versus Δt for the case where the trap with atoms was held on during the laser-pulse firings. (*a*) Comparison during the first 50 μs where the delay was stepped in increments of 1 μs. (*b*) Comparison of the TDGP signal with the measured signal envelope over the full delay range to 500 μs. The TDTF model gives essentially the same envelope. The experimental points have been normalized to unity at short times.

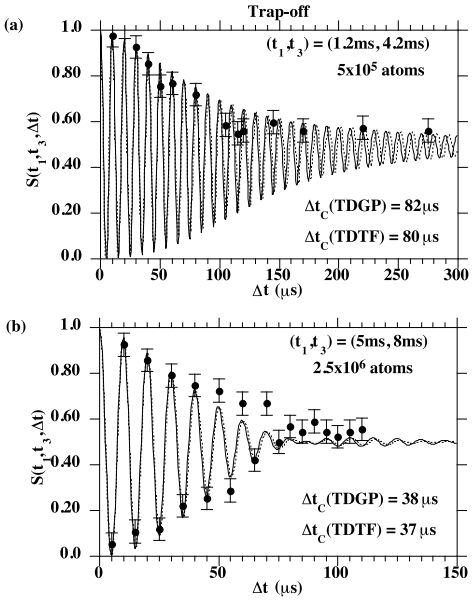

Figure 2. Comparison of TDGP (solid curve) and TDTF (dashed curve) signal functions $S(t_1, t_3, \Delta t)$ with the data (points) for the case where the trap potential was turned off at $t = 0$. (*a*) $(t_1, t_3 = (1.2\ \text{ms}, 4.2\ \text{ms})$ for 5×10^5 atoms in the trap. (*b*) $(t_1, t_3) = (5\ \text{ms}, 8\ \text{ms})$ for 2.5×10^6 atoms in the trap. The experimental points have been normalized to unity at short times.

$$\left(\frac{\partial}{\partial t} - (-2\bar{h}\boldsymbol{k}/m)\cdot\boldsymbol{\nabla} + \frac{\mathrm{i}}{\bar{h}}\left(\frac{-\bar{h}^2}{2m}\nabla^2 + V(\boldsymbol{r},t)\right)\right)\varphi_{-1}$$
$$= -\frac{\mathrm{i}}{\bar{h}}U_0 N(|\varphi_{-1}|^2 + 2|\varphi_0|^2 + 2|\varphi_1|^2)\varphi_{-1}. \tag{16}$$

These equations assume that the condensate wavepackets are normalized so that $\sum_{l=-1}^{1}\int \mathrm{d}\boldsymbol{r}|\varphi_l|^2 = 1$. We use a standard Fourier transform split-operator method for propagating these coupled equations in three dimensions, given the initial conditions generated by equation (10). In practice, a numerical grid of 64 points spanning ± 2 TF radii in each orthogonal direction gives excellent numerical accuracy. The contrast function in equation (2) is calculated from the numerical wavepackets represented as in equation (12).

4. Comparison of theory and experiment

Figure 1 compares the calculated results for $S(t_1, t_3, \Delta t)$ with the NIST data [14] for the case where the trap was held on. In each panel the experimental signal is plotted against the delay Δt used for the first pair of pulses. The signal was measured for Δt in 1 μs increments up to $\Delta t = 50$ μs after which the increment was 30 μs up to $\Delta t = 530$ μs. Figure 1(*a*) shows excellent agreement with the short-time data, which were normalized to unity at the first peak

at 10 μs. The TDGP and TDTF calculations also agree well, except that the phase of the latter slightly lags behind that of the former because of the small acceleration of the fast wavepackets by the effective potential provided by the parent condensate. The long-time evolution of the signal envelope agrees very well between the TDGP and TDTF calculations. The coherence time Δt_c predicted by the two models, around 275 μs, is slightly longer than the measured value of 225 ± 40 μs. When the trap is on, the decay of $S(t_1, t_3, \Delta t)$ is simply due to the reduction of the time-dependent overlap of the moving outcoupled wavepackets. Consequently, the calculated and measured coherence lengths, $\Delta z_c = v\Delta t_c$, are 16 μm and 13 ± 2 μm respectively, about equal to the characteristic size of the parent condensate, $z_{\mathrm{TF}} = 22$ μm. This also implies that coherence extends essentially across the entire outcoupled wavepacket: i.e., the wavepacket has a spatially uniform phase. This result is consistent with a recent investigation of the coherence of a static condensate using Bragg spectroscopy [19].

Figure 2 compares the experimental data for $S(t_1, t_3, \Delta t)$ with the TDGP and TDTF calculations for two cases for which the trap was turned off at $t = 0$. In figure 2(*a*), $(t_1, t_3) = (1.2\ \mathrm{ms},\ 4.2\ \mathrm{ms})$, whereas in figure 2(*b*), $(t_1, t_3) = (5\ \mathrm{ms},\ 8\ \mathrm{ms})$. The data points are normalized to unity as $\Delta t \to 0$. The agreement between the two calculations, as well as the agreement between experiment and theory, is good for both cases. The coherence times and lengths are much smaller for these trap-off cases than for the trap-on case in figure 1. For figure 2(*a*) the respective TDGP and TDTF Δt_c are 82 and 80 μs as compared with 65 ± 10 μs for the experiment. For figure 2(*b*) the corresponding theoretical values of 38 μs and 37 μs compare with a measured value of 45 ± 10 μs. The respective coherence lengths for the (1.2 ms, 4.2 ms) and (5 ms, 8 ms) cases are 5 μm and 2 μm, much smaller than z_{TF}. Since Δz_c is substantially smaller than the condensate size, wavepacket separation is not the only source of signal decay.

The high rate of signal decay when the trap is off is due to the particle interactions that give rise to the nonlinear term in the GP equation. When the trap potential is removed, the parent condensate experiences the effective potential $NU_0|\Psi_0|^2$, which causes the condensate to expand. This causes phase modulation to develop across the condensate, which is associated with an increased spread in the condensate momentum distribution. For example, figure 1 of [14] shows the spatial oscillations in Re (Ψ_0) and Im (Ψ_0) due to this phase modulation. The presence of these oscillations in $\Psi_0(\boldsymbol{r}, t)$ spoil the wavefunction overlap when packet 1 is translated by Δz during the interval Δt, and lead to a much faster loss of coherence between the packets than for the trap-on case. This coherence loss does not represent decoherence due to interactions with an enviroment, but is a consequence of the reduced interference between the packets that results from the spatially dependent phase evolution of $\Psi_0(\boldsymbol{r}, t)$. The longer t_1 is, the greater the coherence loss will be. Since the characteristic time scale to reach terminal momentum spread is $1/\bar{\omega} = 8$ ms, much coherence loss is to be expected for the example in figure 2(*b*).

In conclusion, outcoupled wavepacket coherence times and lengths predicted by solving the 3D SVEA to the TDGP equation are in excellent agreement with data from a recent experiment which measured coherence properties of outcoupled atom-laser wavepackets. The results of the 3D TDTF model are also in good agreement with the SVEA results and the experimental data. Since the outcoupled wavepackets are copies of the parent condensate, the experiment probes both the coherence of the parent condensate as well as that of the outcoupled wavepackets. Spatial and temporal coherence is maintained across the parent condensate while the trap is left on, but is rapidly lost when the trap is turned off, due to phase modulation which develops across the condensate.

Acknowledgments

This work was supported by the US–Israel Binational Science Foundation, the James Franck Binational German–Israel Programme in Laser–Matter Interaction (YBB), the Office of Naval Research, NASA, and by NSF grant no PHY–9802547. The authors would like to acknowledge stimulating discussions with K Burnett.

References

[1] Anderson M H, Ensher J R, Matthews M R, Wieman C E and Cornell E A 1995 *Science* **269** 198
[2] Davis K B, Mewes M-O, Andrews M R, van Druten N J, Durfee D S, Kurn D M and Ketterle W 1995 *Phys. Rev. Lett.* **75** 3969
[3] Bradley C C, Sackett C A and Hulet R G 1997 *Phys. Rev. Lett.* **78** 985
see also Bradley C C, Sackett C A, Tollett J J and Hulet R G 1995 *Phys. Rev. Lett.* **75** 1687
[4] Andrews M R, Townsend C G, Miesner H-J, Durfee D S, Kurn D M and Ketterle W 1997 *Science* **275** 637
[5] Hagley E W, Deng L, Kozuma M, Wen J, Helmerson K, Rolston S L and Phillips W D 1999 *Science* **283** 1706
[6] Band Y B, Trippenbach M and Julienne P S 1999 *Phys. Rev.* A **59** 3823
Japha Y, Choi S, Burnett K and Band Y B 1999 *Phys. Rev. Lett.* **82** 1079
[7] Edwards M, Griggs D A, Holman P L, Clark C W, Rolston S L and Phillips W D 1999 *J. Phys. B: At. Mol. Opt. Phys.* **32** 2935
[8] Mewes M-O, Andrews M R, Kurn D M, Durfee D S, Townsend C G and Ketterle W 1997 *Phys. Rev. Lett.* **78** 582
[9] Bloch I, Hänsch T W and Esslinger T 1999 *Phys. Rev. Lett.* **82** 3008
[10] Kozuma M, Deng L, Hagley E W, Lutwak R, Wen J, Helmerson K, Rolston S L and Phillips W D 1999 *Phys. Rev. Lett.* **82** 871
[11] Ballagh R J, Burnett K and Scott T F 1997 *Phys. Rev. Lett.* **78** 1607
Naraschewski M, Schenzle A and Wallis H 1997 *Phys. Rev.* A **56** 603
Steck H, Naraschewski M and Wallis H 1998 *Phys. Rev. Lett.* **80** 1
[12] Naraschewski M and Glauber R J 1999 *Phys. Rev.* A **59** 4595
[13] Goldstein E V, Zobay O and Meystre P 1998 *Phys. Rev.* A **58** 2373
[14] Hagley E W *et al* 1999 *Phys. Rev. Lett.* **83** 3112
[15] Ovchinnikov Yu B, Müller J H, Doery M R, Vredenbregt E J D, Helmerson K, Rolston S L and Phillips W D 1999 *Phys. Rev. Lett.* **83** 284
[16] Dalfovo F, Giorgini S, Pitaevskii L P and Stringari S 1999 *Rev. Mod. Phys.* **71** 463
[17] Meystre P and Sargent M III 1991 *Elements of Quantum Optics* 2nd edn (New York: Springer) p 171
[18] Kagan Yu, Svistunov B V and Shlyapnikov G V 1996 *Phys. Rev.* A **54** R1753
Castin Y and Dum R 1996 *Phys. Rev. Lett.* **77** 5315
Kagan Yu, Surkov E L and Shlyapnikov G V 1997 *Phys. Rev.* A **55** R18
[19] Stenger J, Inouye S, Chikkatur A P, Stamper-Kurn D M, Pritchard D E and Ketterle W 1999 *Phys. Rev. Lett.* **82** 4569